Stretching effects on the permeability of water molecules across a lipid bilayer

Alain Gauthier and Béla Joós
Ottawa-Carleton Institute for Physics, University of Ottawa Campus, 150 Louis Pasteur, Ottawa, Ontario K1N-6N5, Canada

(Received 29 May 2007; accepted 29 June 2007; published online 12 September 2007)

Using a coarse grained molecular dynamics model of a solvent-surfactant system, we study the effects of stretching on the permeability of water across a lipid bilayer. The density profile, free energy profile, diffusion profile, and tail ordering parameter were computed for a set of stretched membranes maintained at constant area. We computed the water permeability across each membrane using the inhomogeneous solubility-diffusion model first proposed by Marrink and Berendsen [J. Phys. Chem. **98**, 4155 (1994)]. We find that even though the resistance to permeation profile shows a great deal of qualitative change as the membranes are stretched, the overall permeability remains nearly constant within the relevant range of stretching. This is explained by the fact that the main barrier to permeation, located in the densest section of the tails, is insensitive to increased area per lipid, as a result of competing effects. Expansion leads to thinning and a higher density in the tail region, the latter leading to an increase in the free energy barrier. However, this is compensated by the reduction in the transverse distance to cross and a larger diffusion coefficient due to increased disordering in the chains. © *2007 American Institute of Physics*. [DOI: 10.1063/1.2764079]

I. INTRODUCTION

Lipid bilayers (LBs) form the barriers of all cell membranes. In recent years, LBs have attracted interest from diverse fields due to their unique material properties. Lipids are amphiphilic molecules which self-assemble into bilayers in aqueous solutions. The dominant function of the LB in cells is to act as a selective permeation barrier to small molecules, blocking out ions while allowing passage to small nonpolar and polar molecules such as water.[1] It is widely accepted that passive permeation of small uncharged molecules through the LB occurs by a solubility-diffusion process and through transient pores.

In the case of water permeation, there has been some debate as to the role of pores in passive transport. In the mid-1990s, two experimental studies reported somewhat conflicting results on the subject. In their study, Paula *et al.*[2] measured the effect of lipid tail length on the membrane water permeability and fitted both a pore model and a solubility-diffusion model to the data. They found that the solubility-diffusion model fit their data quite well, whereas the pore model underestimated the permeability by several orders of magnitude. This led to the conclusion that water permeates the membrane mostly by a solubility-diffusion process. Recent computer simulations support this conclusion, having found that the pore contribution to water permeability is seven orders of magnitude lower than that predicted by the solubility-diffusion model.[3]

However, results of Jansen and Blume[4] do not support these findings. They found that pores were the main contributor to water permeation. Paula *et al.* attribute the conflicting results to two important differences between the experiments.[2] First, Jansen and Blume used saturated lipid vesicles, whereas Paula *et al.* used unsaturated lipid vesicles. Experiments have shown that membranes composed of unsaturated lipids are more permeable to water and have lower chain ordering than those composed of saturated ones.[5–7] The second difference between the two studies is that Jansen and Blume used an outward concentration gradient, whereas Paula *et al.* used an inward concentration gradient.[2] In the case of an outward concentration gradient the LB would initially be stretched and water would flow outward from the vesicle interior. This tension on the LB produces an area expansion, which would favor pore formation. Jansen and Blume used small tensions, staying well below the rupture point found to occur at 4% extension.[4,6,8–10] A recent experimental study has reported that a small stretch has little or no effect on LB permeability. Vitkova *et al.* found only a slight increase in the permeability as the tension on the LB was increased.[11]

Stretching effects on the structure of the LB and its effects on the permeability of water remain somewhat misunderstood. In this article, we examine how the permeability of the LB changes with increased area per lipid. Our focus is on small pore free LBs, as we calculate the LB's resistance to permeation R_p. We use a coarse grained molecular dynamics simulation to model a LB in water and to calculate the permeability using the inhomogeneous solubility-diffusion model (ISDM) first proposed by Marrink and Berendsen.[12] This model relates the molecular flux through a membrane to an applied thermodynamic gradient,

$$J = -\frac{c^* \Delta\mu}{R_p RT}, \tag{1}$$

where c^* is the equilibrium water concentration in the bulk, $\Delta\mu$ is the thermodynamic gradient on either side of the membrane, R is the gas constant, T is the temperature, and R_p is

the permeation resistance. R_p is obtained from the local permeation resistances $R(z)$ as follows:

$$R_p = \int_{z_1}^{z_2} R(z)dz = \int_{z_1}^{z_2} \frac{\exp(\Delta G(z)/RT)dz}{D(z)}, \quad (2)$$

where $\Delta G(z)=G(z)-G(z^*)$ is the free energy difference at position z within the membrane with respect to the bulk, $D(z)$ is the one dimensional diffusion coefficient at position z along the membrane normal, and z_1 and z_2 are positions in the bulk on either side of the membrane. This approach has been extensively used in recent years to examine the permeability of different sized solutes,[13–16] lipid tail branching effects on permeability,[17] as well as lipid tail length.[18] The resistance to permeation is related to the experimentally observed permeability coefficient by $R_p=1/P$.[12]

To see the connection to simpler models and a greater insight into Eq. (2), one can note that if the membrane is approximated as a homogeneous medium, such as a layer of oil, then $\Delta G(z)$ and $D(z)$ do not depend on z and the ISDM reduces to

$$R_p = \frac{\exp(\Delta G/RT)}{D}\int_{z_1}^{z_2} dz = \frac{d}{DK}, \quad (3)$$

where D is the diffusion coefficient of the permeant within the membrane, $K=\exp(-\Delta G/RT)$ is the solute partition coefficient measuring the barrier to enter the membrane, and d is the membrane thickness. This limit of the ISDM is known as the homogeneous solubility-diffusion model (HSDM), which relates the permeability of water to the diffusion and partition coefficient as $P=DK/d$.[19]

The article is divided as follows. In the next section, we describe our ISDM approach in greater detail, first describing the coarse grained model, the methods used to obtain the diffusion and free energy profiles, and the stretching method. In Sec. III we present our results on the structural changes with stretch, changes in the profiles, and finally changes in the permeability. We conclude the article with a summary of our results.

II. METHODS

A. The coarse grained molecular dynamics model

In our study, we use the coarse grained molecular dynamics model developed by Goetz and Lipowsky[20] to simulate a LB/water system. This is a versatile model that has been used to study LB elasticity,[20] bending in LBs,[21,22] the lateral diffusion of lipids within a monolayer,[23] and pore formation.[24,25] In this model, lipid and water molecules are approximated using beads of three types: water beads (W), hydrophilic beads (H), used to model lipid heads, and hydrophobic beads (T), used to model the tails. Particles which have the same hydrophilicity interact with a Lennard-Jones potential $U_{\mathrm{LJ}}(r)=4\epsilon[(\sigma/r)^{12}-(\sigma/r)^6]$, whereas those with differing hydrophilicity interact with a softcore repulsive potential $U_{\mathrm{SC}}(r)=4\epsilon(\sigma_{\mathrm{SC}}/r)^9$, where $\sigma_{\mathrm{SC}}=1.05\sigma$. All intermolecular interactions were cut off at 2.5σ, and the potentials were shifted in such a way that $U_{LJ}(r)$ and $U_{\mathrm{SC}}(r)$ are continuous at the cutoff value.

The lipids are held together by a harmonic spring potential, which is applied to the ith and $(i+1)$th beads along a lipid $U_{\mathrm{HP}}(r_{i,i+1})=k_2(|r_{i,i+1}|-\sigma)^2$. Stiffness within a lipid is obtained using a three body bond angle potential $U_{\mathrm{BA}}(\phi_i)=k_3(1-\cos(\phi_i-\phi_i^{\mathrm{sp}}))$. The angle preference combined with the relaxed bond length determines the relaxed shape of the lipid. In all our simulations, we set $k_2=5000\epsilon$ and $k_3=2\epsilon$ and used the same angular preference as in Ref. 20. Lipids were modeled as $H_3(T_6)_2$ (i.e., a three particle head and two six particle tails), which gives an appropriate ratio of 15:1 between the relative sizes of a lipid and a water particle. Following Goetz and Lipowsky,[20] estimates for the real physical quantities are obtained by using $\epsilon=2$ kJ/mol, $\sigma=1/3$ nm, and $m=36$ g/mol. Therefore, a T bead represents about three to four monomers and a W bead represents one to two water particles. This model is described in Ref. 20, except for the lipid architecture which has longer tails: we use six tail particles instead of four to have similar density profiles as in published atomistic models of a common biological lipid dipalmitoylphosphatidylcholine (DPPC) (see for instance, Refs. 12 and 27), in particular, the small dip near the center of the LB, which is not seen with shorter chains (see Fig. 2).

Bilayers were preassembled by randomly placing an equal number of lipids in each monolayer at the center of the simulation box and filling the remainder of the box with randomly placed water beads. The system was then relaxed for approximately 10^4 Monte Carlo steps, followed by 2×10^6 molecular dynamics steps, corresponding to about 1.5 ns with the above conversion. All simulations were done in the NVT ensemble, where N is the total number of particles, V the volume of the system, and T its temperature. The overall system density is kept at $2/3\sigma^3$. In all our simulations, we used 110 lipids and $n=3348$ water molecules giving a simulation cell volume of $7497\sigma^3$. The temperature was maintained constant at $RT=1.35\epsilon$ (which corresponds to 324 K) through a Nose-Hoover algorithm. New positions and velocities were found using the Verlet leapfrog algorithm.

B. Calculating the permeability

The permeability was calculated using the ISDM first proposed by Marrink and Berendsen,[12] as given by Eq. (1). Recalling Eq. (2),

$$R_p = \int_{z_1}^{z_2} \frac{\exp(\Delta G(z)/RT)dz}{D(z)}, \quad (4)$$

we can obtain the permeability by calculating both $\Delta G(z)$ and $D(z)$. Two strategies were used, depending on the probability of passage of the water beads. In regions where the W beads visit on the time scale of the simulation, we can use the system particles to obtain both $\Delta G(z)$ and $D(z)$. The probability of finding a water particle at position z with respect to the bulk $P(z;z^*)=c(z)/c(z^*)$ is given by

$$P(z;z^*) = \frac{\int dV^{3N-n} \int dz'^n \delta(z'-z) e^{-(U+PV)/RT}}{\int dV^{3N-n} \int dz'^n \delta(z'-z^*) e^{-(U+PV)/RT}} = e^{\Delta G(z)/RT}. \tag{5}$$

Rearranging, we get

$$\Delta G(z) = RT \ln(c(z)/c(z^*)). \tag{6}$$

Therefore, the free energy profile can be obtained from the concentration profile [or density profile $n(z)$] of water particles along the LB normal. We use this method in regions where the average density of the particles is greater then 20% of the bulk density.

The diffusion coefficient in these same regions can be obtained from the mean squared displacement of the W bead in the neighborhood of the position z,

$$D(z) = \lim_{t\to\infty} \frac{\langle |z(t) - z(0)|^2 \rangle}{2t}. \tag{7}$$

The diffusion coefficient of interest here is the "local" diffusion coefficient, representing movement on a short time scale. We consider the mean squared displacements over a time of 5000 time steps (one time step equals $dt = 0.0005\sqrt{m\sigma^2/\epsilon}$ or $5000dt$ corresponds to about 3 ps). The value of the diffusion constant at a position z was obtained by slicing the simulation box along the LB normal. The mean squared displacements of the beads whose geometric center of displacement is confined between $z-\Delta z$ and $z+\Delta z$ were used to calculate $D(z)$ at z.

A different approach is needed in the interior of the LB where water beads do not visit as often. In these regions, we make use of the force on a constrained W bead, held at a fixed position z_0, to calculate both the diffusion and the free energy profiles. As shown in Refs. 12 and 17, the derivative of the free energy at z_0 is related to the average force of the constrained particle $\langle F_z(z_0) \rangle$ by

$$\frac{d\Delta G(z_0)}{dz} = -\langle F_z(z_0) \rangle. \tag{8}$$

By integrating Eq. (8) and combining with the ΔG profile found using Eq. (6), we obtain the full free energy profile across the LB.

The instantaneous values of the force on the constrained particle can also be used to calculate the diffusion profile $D(z)$ inside the LB. According to the fluctuation-dissipation theorem, the autocorrelation of random forces acting on a molecule is related to the diffusion coefficient by

$$D(z) = \frac{(RT)^2}{\int_0^\infty \langle \Delta F(z,t) \Delta F(z,0) \rangle dt}. \tag{9}$$

The random forces are obtained from the fluctuations of the instantaneous force from the thermally averaged force at time t, $\Delta F(z,t) = F(z,t) - \langle F(z,t) \rangle$.

During a simulation, we placed W beads at different depths in the LB and constrained them to lie in the plane $z = z_0$ for the duration of the simulation. The constrained particles interact with the surrounding beads and are free to diffuse in the xy plane. At each iteration, we rescaled the system positions so that the center of mass of the LB is kept fixed in the center of the simulation box. This ensures that the distance between the constrained particle and the center of mass of the LB is constant. A similar technique is discussed in Refs. 12 and 14. The initial insertion of the constrained particle was done in such a way as not to "shock" the system. If a particle is naively inserted randomly into the LB, it may be placed unphysically close to other particles and cause an overestimate of the force. To avoid this, the interaction potential of 100 random sites in the z_0 plane was tested, while the system was kept still. Each insertion was relaxed for 10^3 iterations in the fixed configuration using a steepest decent minimization. The test bead with the lowest energy out of the sample of 100 was selected for the constrained particle method. We then relax the system containing the inserted bead for 10^4 iterations. A total of 18 z_0 positions along the LB normal allowed us to obtain a good profile inside the LB.

C. Stretching method

The stretching procedure was done in such a way as to simulate a quasistatic isochoric process. This was achieved by initializing a series of stretched LBs, all in the same NVT ensemble. Each LB was stretched by extending the simulation box in the xy direction, while compressing it along the z direction so as to conserve the total volume. These were then relaxed and thermalized, as described in Sec. II A. This gives us a set of LBs each characterized by an area per lipid. The tensionless area per lipid a_0, which corresponds to a LB in the tensionless state, is used as our reference. The stress of the LB is related to the area per lipid through

$$\Sigma = K_A \frac{(a-a_0)}{a_0}, \tag{10}$$

where Σ is the interfacial tension, a is the area per lipid, and K_A is the compressibility modulus. If $\Sigma < 0$ we say that the LB is compressed, and if $\Sigma > 0$ we say that the LB is stretched. The value of Σ is calculated from the stress profile $s(z)$, along the LB normal,

$$\Sigma = \int_{-\infty}^{\infty} s(z) dz, \tag{11}$$

where $s(z) = \Sigma_z(z) - 0.5 \cdot (\Sigma_x(z) + \Sigma_y(z))$ is the difference between the normal and lateral stresses. The values $\Sigma_x(z)$, $\Sigma_y(z)$, and $\Sigma_z(z)$ are obtained from the thermal averaging of the microscopic stress tensor $\sigma^{\alpha\beta}(z)$, as described in Ref. 20.

Figure 1 shows the resulting stress Σ as a function of the area per lipid, obtained using Eq. (11). A linear behavior is observed for small extensions. Also shown is a linear fit near the tensionless state, from which we obtain the values of a_0 and K_A [viz., Eq. (10)]. At larger extensions, we find a sublinear behavior similar to that found by the authors in Ref. 20 for the $H_3(T_4)_2$ LB. In Table I we present these values and compare them to typical experimental values.[26] Both a_0 and K_A are of the same order of magnitude as those obtained from experiment. The tensionless thickness of the LB d_{t0} is defined as the distance between the maxima of the head particle distributions.

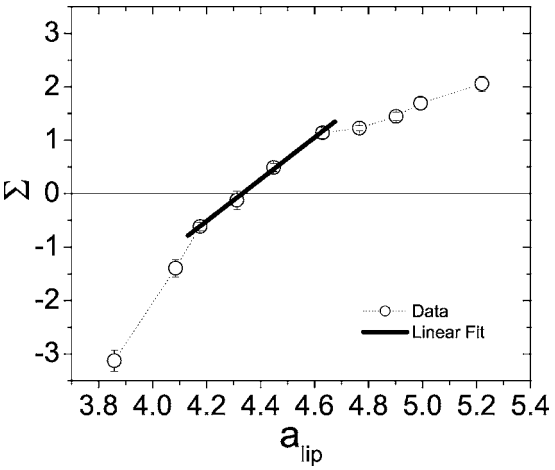

FIG. 1. Stress as a function of the area per lipid. Values of the slopes and y intersection obtained from the linear fit (dashed line) were used to obtain the values of K_A and a_0 given in Table I.

Of note here is that these simulated LBs can support stresses well above the rupture point of real LBs, $\Delta a/a_0 = 4\%$. A recent numerical study[25] has shown that at the maximum expansion a simulated LB can support before it ruptures scales as $\Delta a/a_0 \sim N_{\mathrm{lip}}^{-1/3}$. This scaling relation suggests that a LB composed of about 10^2 lipids can support extensions up to 20% without rupture. At such high extensions, the lipids in LBs must undergo substantial rearrangement in order for the LB to stay intact.

III. RESULTS

A. Stretching effects on bilayer structure

With increased area per lipid, the LB undergoes substantial changes in structure. To quantify these changes, we looked at the density profile of the lipid and present it in Fig. 2. In order to more clearly describe the changes which occur during stretching, we divide the LB into four parts similar to what is done in Ref. 12. We used both the density profile and the average force on a constrained particle to define the boundaries, as described in the Appendix. This provides a means to compare with atomistic simulations. The four regions are region 1 which represents W and feels the presence of the LB, region 2 the hydrophilic interphase, region 3 the hydrophobic interphase, and region 4 the LB interior.

In the tensionless state, we observe the highest overall bead density in region 3 just behind the head beads and a global minimum in region 2. A local minimum in the total density is observed at the center of the LB. The shape of the profile is somewhat different from results found using atomistic simulations. In atomistic simulations, regions 2 and 3 have similar density and the global minimum is usually found in the center of the LB.[12,27,28] In our simulations, the average amount of W and T beads which penetrate into region 2, the H dominated section of the LB, is very low. This is an artifact due to the simplicity of the soft core potential U_{sc} used to model the hydrophobic-hydrophilic interactions (see Sec. II A). On average, tail and water beads stay approximately 2σ apart. More sophisticated potential functions incorporating different length scales should reduce this artifact drastically and would produce a more realistic region 2.

TABLE I. Comparison of the values of area compressibility modulus K_A, the tensionless area per lipid a_0, and the total thickness of the model LB d_{t0}, defined as the distance between the heads, as compared with the equivalent quantities for typical LBs obtained from experiment converted to our units (Ref. 26).

Lipid	K_A (ϵ/σ^2)	a_0 (σ^2)	d_{t0} (σ)
$H_3(T_6)_2$	16.99±0.47	4.34±0.10	8.70±0.5
Expt.	7.2 (240 mN/m)	5.85 (0.65 nm^2)	10.5 (3.5 nm)

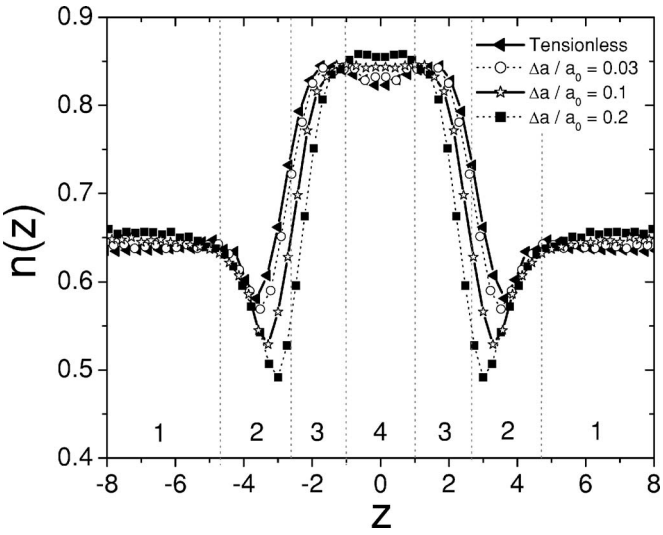

FIG. 2. Effects of stretching on the total density across the LB. The boundaries displayed for the four regions defined in Sec. III A and the Appendix are those of the tensionless state (dotted vertical lines).

As the LB is stretched, we observe that the density changes most substantially in regions 2 and 4. In region 2 the total density decreases while the dip in density in region 4 is almost nonexistent at larger stretch values. As the area per lipid increases, region 3 remains nearly unaffected but shifts to the center of the LB. The electron density profiles of the atomistic models of Feller *et al.* performed in a *NAPT* ensemble also found that increased area leads to little change in the region just behind the head sections (our region 3), whereas the "dip" of region 4 was found to increase and disappear. Their model did not show a decrease in density in region 2.[27,28]

From the density profiles, the effects of stretch on LB thickness were studied (see Fig. 3). The total thickness of the LB d_t is defined as the distance between the maxima of the head particle distributions. From Fig. 3 it is clear that the area per lipid and the LB thickness are linearly related. If the membrane was incompressible then the changes in area per lipid and in the thickness of the membrane would be related by $\Delta a/\Delta d_t = a_0/d_{t0}$.[29] We can rewrite this expression as $d = d_{t0} - d_{t0}(\Delta a/a_0)$, where d_{t0} is the tensionless thickness. From a linear fit of the inset of Fig. 3 we find that $d = (8.44\pm0.06) - (6.42\pm0.46)(\Delta a/a_0)$. Note that the intercept agrees very well with the value of the thickness $d_{t0} = 8.70\pm0.5$ but that the slope is smaller than expected for an incompressible fluid.

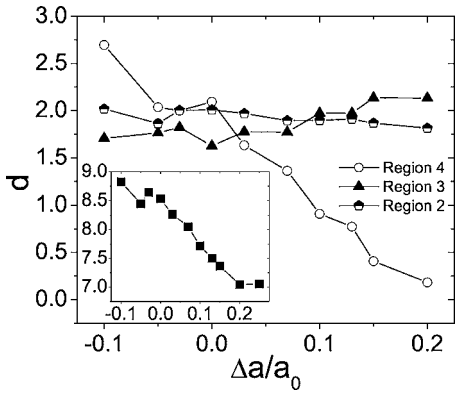

FIG. 3. Decrease in the thickness of the various regions (see Sec. III A) in the LB as a function of LB extension. Shown in the inset is the decrease in the total thickness d_t as a function of stretch.

Dividing each density profile in terms of the three boundaries defined above, we can observe how different parts of the LB compress as the area per lipid increases. Figure 3 shows that region 4, the center of the membrane, undergoes the most significant reduction in thickness, while regions 2 and 3 remain at about the same thickness. The interior of the membrane behaves as a compressible fluid. The lipid tails rearrange themselves in such a way as to preserve both the hydrophobic and hydrophilic interphases at the expense of region 4.

Given that the LB thins as the area per lipid increases, the next question to ask is how the lipid tails rearrange themselves. To examine this question further, we calculated the order parameter for the chains,

$$S_{\mathrm{CD}} = \tfrac{1}{2}(3\cos^2\langle\theta\rangle - 1). \tag{12}$$

Ordered segments will have values close to −0.5 when perpendicular to the LB normal and 1 when parallel to the LB normal. Unordered bonds will have $S_{\mathrm{CD}} \sim 0$. We distinguish each bond by labeling them with a number. The head of the lipid is composed of three particles connected by two bonds, 1 and 2. The tail bonds are labeled going down the lipid, where 3 corresponds to the head-tail bonds and labels 4–8 correspond to the remaining tail segments. We averaged the S_{CD} values for each tail.

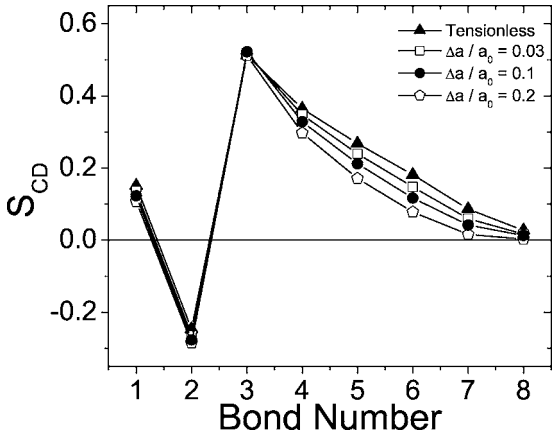

FIG. 4. The stretching effects on the ordering of the lipid bonds. Note the decrease in the ordering of the tail bonds with extension.

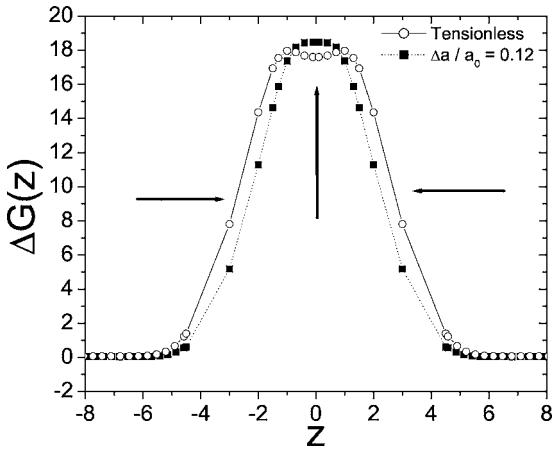

FIG. 5. Stretching effects on the free energy profiles. Arrows show how the profile changes with increased area per lipid. At high stretch values, the "dip" in the center of the lipid bilayer (LB) disappears.

Figure 4 shows that the ordering of the tails decreases with increasing area per lipid. The head and first *H-T* bonds are affected very little by the increased area per lipid. The bonds that see the most change are the ones that correspond to region 3. Stretching reduces the ordering of the lipid tail ends. At high stretch values, region 4 disappears and the LB can be considered as being composed of the hydrophobic interface (region 3–region 3) and hydrophilic interfaces (region 1–region 2). The results of Feller *et al.* using atomistic simulations showed a similar decrease in tail ordering with increased area per lipid.[27,28]

B. Diffusion and free energy profiles

Given the structural changes which occur with increased area per lipid, we expect that both the diffusion and free energy profiles should show changes as the LB is stretched. In Figs. 5 and 6 we present free energy and diffusion profiles in the tensionless state as well as at 12% extension. Stretch has two main effects on the free energy profile, a narrowing of the profile and a reduction in the depth of the dip in region 4. The thinning of the LB comes at the expense of increased density in the center of the LB. At increased density, particles

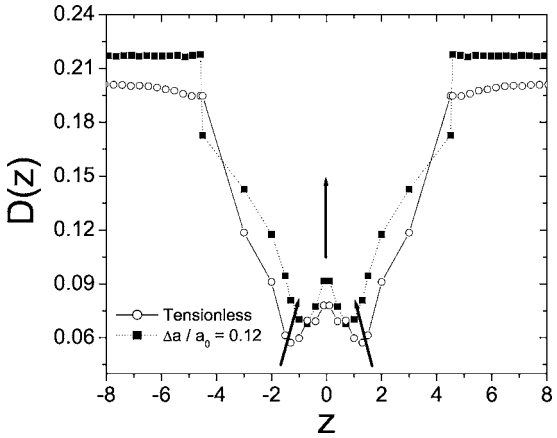

FIG. 6. Stretching effects on the diffusion profile. As the LB is stretched, the diffusion coefficient in the LB interior increases and the profile is also seen to narrow (as shown by the arrows).

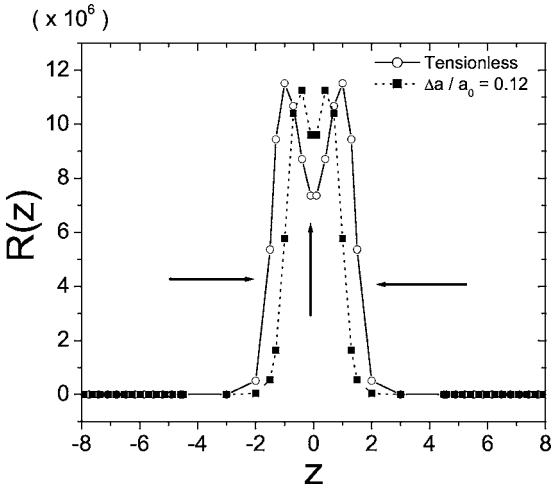

FIG. 7. Stretching effect on the resistance to permeation of the LB. Arrows indicate how the profile is changing with increasing area per lipid. Error bars are omitted for clarity.

in region 4 surrounded by T beads will be subject to higher forces thus leading to an increase in the free energy in the center of the LB. This trend continues until region 4 disappears, $\Delta a/a_0 > 20\%$ at which point we observed that our LBs were unstable.

Diffusion along the LB normal is mostly affected near the center of the LB. Similar to the free energy profiles, the diffusion profiles become much more narrow as the LB is stretched. Surprisingly, $D(z)$ in both regions 3 and 4 increase despite an increase in the overall density in these parts of the LB. The higher diffusion coefficient observed in these regions at increased stretch is most likely due to the increase in free volume found in these parts of the LB. Because of the decrease in tail ordering, we expect larger free volume pockets to become more probable, thus facilitating diffusion.[33] These trends continue up to about $\Delta a/a_0 > 20\%$ at which point no "hump" in the diffusion profile is apparent, and D_z in regions 3 and 4 of the LB are characterized by a single diffusion coefficient.

C. Stretching effects on the resistance to permeation and permeability

Combining the free energy and diffusion profiles allows us to obtain the resistance to permeation profile. In Fig. 7 we show profiles of both the tensionless and $\Delta a/a_0 = 12\%$ stretched states. The $R(z)$ profile in the tensionless state has a very similar shape to those found in Ref. 14. Our $R(z)$ maximum is equal to $11.5 \pm 6.0 \times 10^6 \sqrt{m/\epsilon\sigma^2}$ leading to a permeability $P = 4.42 \pm 2.4 \times 10^{-7} \sqrt{\epsilon/m}$, corresponding to approximately 11.0 ± 6.0 μm/s (at 324 K) with the conversion suggested in Sec. II B. There is, however, a significant degree of flexibility in the conversion from the coarse grained model to real values.[20]

Experimental values of the water permeability of lipid bilayers in the liquid crystalline phase vary over three orders of magnitude depending on temperature, experimental procedure, and lipid structure: from 10 to 10^3 μm/s at biological temperatures (303–315 K) for DPPC membranes.[2,6,30] The most recent of the quoted experimental measurements on polyunsaturated PC bilayers yielded permeabilities between 28 and 146 μm/s depending on the lipid tail structure.[6] Vesicles containing lipids from archaebacteria membranes have been found to have much lower values of water permeability from 4.9 to as low as 0.4 μm/s.[31] Our value of P lies within the lower range of these values. Atomistic simulations for the DPPC lipid bilayer permeability have found values of 133 ± 28 μm/s (323 K) (Ref. 14) and 700 ± 300 μm/s (350 K),[12] about one order of magnitude higher than our value.

Applying stretch to the LB causes the width at the base of the $R(z)$ profile to thin. The $R(z)$ values in region 4 increase, as indicated by the arrows in Fig. 7. This follows the trend observed in the case of the free energy profile. The increase in the diffusion coefficients in regions 3 and 4 slows the increase of the $R(z)$ values in these regions. At high stretch values, the profile has a Gaussian shape (no dip at the center of the LB) consistent with the disappearance of region 4. The changes in the resistance to permeation profile as a function of stretch are qualitatively similar to reducing the tail length. Sugii *et al.* reported that the width of the $R(z)$ profiles thins with decreasing tail length. They also observe a reduction of the dip in $R(z)$ for the LB composed of shorter tailed lipids.[18] The similarities are only qualitative, however, as they report a substantial decrease in the maximum value of the $R(z)$ profile with decreasing tail length.

By using Eq. (2) to calculate the permeability, we implicitly assume that the thermodynamic gradient has fluctuations of the order of RT over the correlation distance of the water particle.[12] This assumption comes into question in region 2 where ΔG increases significantly. Following the method in Ref. 14 we calculate the largest variation in the free energy to verify that $\Delta G \leqslant RT$ in this region. The mean displacement of the particle is given by $d_{\mathrm{corr}} = 2D(z)t_{\mathrm{corr}}$, where t_{corr} is the correlation time of the force autocorrelation function given in Eq. (9). The longest correlation time found in the membrane interior was of a few hundred iterations,[32] $t_{\mathrm{corr}} \approx 0.15\sqrt{m\sigma^2/\epsilon}$. An upper bound for the diffusion coefficient $D(z)$ in region 2 is approximately $0.1\sqrt{\epsilon/m\sigma^2}$, which gives a correlation distance $d_{\mathrm{corr}} = 0.17\sigma$. From Fig. 5, we can interpolate a variation ΔG over d_{corr} of $\approx 1.11\epsilon$, which is smaller than $RT = 1.35\epsilon$. Therefore even in the worst case scenario, ΔG is still below RT so the barrier ΔG can be overcome by thermal fluctuations and the motion is in general diffusive.

Not shown on the graphs of Fig. 7 are the error bars, which are calculated using the standard deviation of, no less than 5 and up to 8, independent runs at each stretch value. Although these are quite substantial in absolute terms (about 50%–100% of the values depending on z), the effect of stretch on each sample is shown by the arrows in the figure. The large error is a consequence of the use of the average force on a constrained particle. Other works have avoided such large errors by using the Widom particle insertion method[12,14,17] but due to the higher density of our system, this method did not work with our model LB.

A certain amount of systematic error is also intrinsic in the use of this method. The bending rigidity κ_b in these bilayers is small, about $20k_BT$ using the expression given in

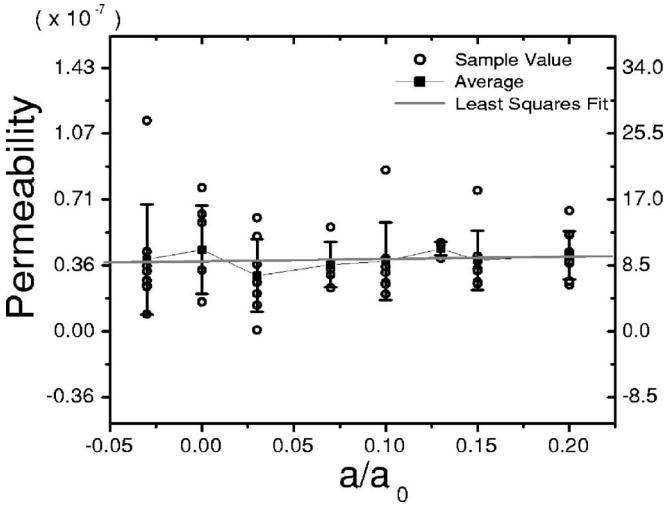

FIG. 8. Stretching effects on the overall permeability of the $H_3(T_6)_2$ LB. The linear fit parameters $y=a+bx$, shown with a straight line, are $a=(3.8\pm0.3)\times10^{-8}$ and $b=(1.2\pm2.4)\times10^{-8}$. The left hand scale is in reduced units while the right hand scale is in μm/s.

Ref. 34 ($\kappa_b=K_A d_{t0}^2/48$). This implies that transverse thermal fluctuations will be significant. The wavelength of these oscillations will be as short as the size of a single lipid and, in simulations, as long as the simulation box. The accuracy of the constrained particle method depends on the fact that the distance of the inserted particle to the center of the simulation cell is fixed. If the LB oscillates about its center of mass, then an inserted particle may stray from its intended position. These waves are known to be more pronounced in the tensionless state.[35] Therefore, we would expect that there be a greater variation when we are near the tensionless state. If transverse waves are present, the constrained particle may migrate to regions of lower free energy along the plane to which it is constrained. Therefore the constrained particle method may underestimate the free energy.

Given the changes observed in the resistance to permeation profile of the LB as it is stretched, at first thought, we would expect to see a significant change in the overall permeability. This is not the case. In Fig. 8, we show the overall permeability of the LB as a function of stretching. The error bars represent the standard deviation of the permeability found from the independent samples. We plot the average as well as the sample distribution. Except for a few stray points, all sample values are of the same order of magnitude.

Experimental data describing the dependence of the permeability on LB stretch is rather limited. To our knowledge, only one recent study has measured this dependence. Our findings are very similar to the results of Vitkova *et al.*;[11] the permeability increases very little with increasing tension. The authors of Ref. 11 argue that, if there is an increase, it would be due to pore formation. From a linear fit of the averaged simulation data presented in Fig. 8, we find an increasing trend in permeability, without any pores being present in the LB.

IV. DISCUSSION

This work has shown that the main barrier to permeation of a LB can be simulated using a simple solvent-surfactant model. The general features of the model agree with atomistic simulations and capture the same essential characteristics of the resistance that a LB offers to a permeating water molecule. Both atomistic simulations and experiments have shown that the main permeation barrier is located just behind the head section in regions 2 and 3.[12,17,36] This is precisely where we find the peak in our resistance to permeation profiles.

Increasing the area per lipid of a LB has significant effects on the LB structure. Specifically, we have found that the density in the LB center significantly increases while the tail ordering in the dense hydrophobic section decreases. The lateral extension is compensated by a compression along the LB normal. Describing the LB in terms of four regions, we found that the compression is done in the center of the LB (region 4), leaving the hydrophilic and hydrophobic interfaces mostly intact. The ends of the tails become increasingly unordered with increased area per lipid, whereas the head and upper part of the tails are much less affected.

Because the structural changes are located in the LB interior, only water molecules within the LB would "feel" these changes. As shown by the free energy profiles region 3 remains the most significant barrier to permeation. The decrease in tail ordering in this region does lead to a slightly higher diffusion coefficient. Therefore, when water molecules penetrate into the LB, they would find an increase in mobility. However, the increase in the diffusion coefficient is compensated by the increase in the free energy barrier and a collapse of region 4. Accordingly, the changes in the diffusion and free energy profiles lead to a change in the shape of the resistance to permeation profile, but the total area remains essentially the same (see Fig. 8), or there is very little change in the overall permeability. Most of the resistance comes from region 3, which shifts inward.

In brief, three structural changes in the LB are occurring during the stretching process, thinning, increasing density, and decreasing tail order. The thinning and decrease in tail ordering combine in such a way as to compensate for the increase in density in the center of the LB.

V. CONCLUSION

This work has shown that a simple solvent-surfactant model presents a very similar barrier to permeation as more sophisticated atomistic simulations. Stretching the LB does not produce any significant change in the permeability. It was found that three effects compensate each other so that the overall permeability remains essentially constant, in agreement with recent experimental observations.[11] Therefore, as the LB is stretched, one does not expect to see an increased amount of water within the LB. There was no need to invoke diffusion through pores to explain the changes or rather lack of a clear change in the permeability with stretching. This makes it likely that when pores form, they do so from the outside surfaces of the LB through transient thermally activated defects.

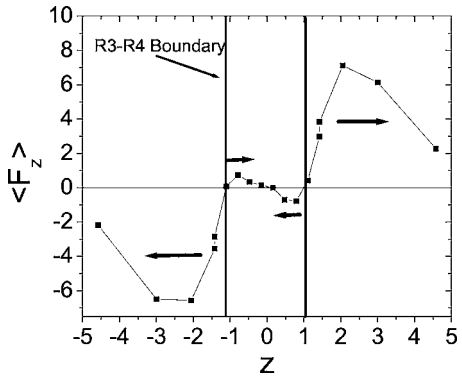

FIG. 9. Plot of the average force on a constrained particle. Arrows indicate the direction in which the particle is accelerated on average. Note the three null force points, two of which are unstable, chosen as the region 3–region 4 (R3-R4) boundaries, and one which is stable at the LB center.

APPENDIX

The boundaries of each section of the LB were chosen to approximate the four regions presented in Ref. 12. The region 1–bulk water boundary (region 1–bulk) was chosen as the point where the water density profile first starts to decrease from the system density (i.e., $\rho=2/3$). The region 1–region 2 boundary was defined as the intersection between the water density profile and the H density profile. This corresponds to the point where the water density is at about half that of the bulk. The region 2–region 3 boundary was defined as the location where the H particle density dips below 1% of the peak value. In this way, region 2 represents the head dominated section of the LB. The region 3–region 4 boundary was somewhat ambiguous. region 4 represents the LB interior; therefore, it should offer a barrier to an escaping particle. From the $d\Delta G/dz=-\langle F_z\rangle$ profile, we get the force exerted by the LB on a water particle across the LB. In the LB interior, the force will either be 0 or directed toward the center of the LB, as shown in Fig. 9. This is due to the lower density at the LB center; on average, the W bead will be further from the T, beads which produces a less significant $\langle F_z\rangle$. Therefore, we observe three fixed null force points, two of which are unstable due to increased density in region 3 and one which is stable at the LB center. We chose the two unstable null force points as our region 3–region 4 boundaries.

ACKNOWLEDGMENTS

The work has been funded by the Natural Sciences and Engineering Research Council (Canada). We also acknowledge generous computer time made available to us on Bugaboo at Simon Fraser University.

[1] B. Alberts, D. Ray, J. Lewis, M. Raff, K. Roberts, and J. D. Watson, *Molecular Biology of the Cell*, 2nd ed. (Garland, New York, 1989).
[2] S. Paula, A. G. Volkov, A. N. Van Hoek, T. H. Haines, and D. W. Deamer, Biophys. J. **70**, 339 (1996).
[3] D. P. Tieleman and S. J. Marrink, J. Am. Chem. Soc. **128**, 12462 (2006).
[4] M. Jansen and A. Blume, Biophys. J. **68**, 997 (1995).
[5] C. Groth, K. Tollgerdt, and M. Nyden, Colloids Surf., A **281**, 23 (2006).
[6] K. Olbrich, W. Rawicz, D. Needham, and E. Evans, Biophys. J. **79**, 321 (2000).
[7] T. X. Xiang and B. D. Anderson, Biophys. J. **75**, 2658 (1998).
[8] L. Fournier and B. Joós, Phys. Rev. E **128**, 051908 (2003).
[9] D. Needham and R. M. Hochmuth, Biophys. J. **55**, 1001 (1989).
[10] E. A. Evans and D. Needham, J. Phys. Chem. **91**, 4219 (1987).
[11] V. Vitkova, J. Genova, and I. Bivas, Eur. Biophys. J. **33**, 706 (2004).
[12] S.-J. Marrink and H. J. C. Berendsen, J. Phys. Chem. **98**, 4155 (1994).
[13] S. J. Marrink and H. J. C. Berendsen, J. Phys. Chem. **100**, 16729 (1996).
[14] D. Bemporad, J. Essex, and C. Luttmann, J. Phys. Chem. **108**, 4875 (2004).
[15] D. Bemporad, J. Essex, and C. Luttmann, Biophys. J. **87**, 1 (2004).
[16] T. X. Xiang and B. D. Anderson, Adv. Drug Delivery Rev. **58**, 1357 (2006).
[17] W. Shinoda, M. Mikami, T. Baba, and M. Hato, J. Phys. Chem. **108**, 9346 (2004).
[18] T. Sugii, S. Takagi, and Y. Matsumoto, J. Chem. Phys. **123**, 184714 (2005).
[19] A. Finkelstein, *Water Movement Through Lipid Bilayers, Pores and Plasma Membranes* (Wiley-Interscience, New York, 1987).
[20] R. Goetz and R. Lipowsky, J. Chem. Phys. **108**, 7397 (1998).
[21] R. Goetz, G. Grompper, and R. Lipowsky, Phys. Rev. Lett. **82**, 221 (1999).
[22] W. K. den Otter and W. J. Briels, J. Chem. Phys. **118**, 4712 (2003).
[23] A. Imparato, J. C. Shillcock, and R. Lipowsky, Eur. Phys. J. E **11**, 21 (2003).
[24] T. V. Tolpekina, W. K. den Otter, and W. J. Briels, J. Chem. Phys. **121**, 12060 (2004).
[25] T. V. Tolpekina, W. K. den Otter, and W. J. Briels, J. Chem. Phys. **121**, 8014 (2004).
[26] W. Rawicz, K. C. Olbrich, T. McIntosh, D. Needham, and E. Evans, Biophys. J. **79**, 328 (2000).
[27] S. E. Feller, R. M. Venable, and R. W. Pastor, Langmuir **13**, 6555 (1997).
[28] S. E. Feller, Y. Zhang, and R. W. Pastor, J. Chem. Phys. **103**, 10267 (1995).
[29] O. Hamill and B. Martinac, Physiol. Rev. **81**, 685 (2001).
[30] A. Carruthers and D. L. Melchior, Biochemistry **81**, 5797 (1983); J. Androsko and S. Forsén, Biochem. Biophys. Res. Commun. **60**, 813 (1974); Y. Graziani and A. Livne, J. Membr. Biol. **7**, 275 (1972); A. Finkelstein, J. Gen. Physiol. **68**, 127 (1976); G. Bacic, R. Srejic, and S. Ratkovic, Stud. Biophys. **138**, 95 (1990).
[31] J. C. Mathai, G. D. Sprott, and M. L. Zeidal, J. Biol. Chem. **279**, 27266 (2001).
[32] A. Gauthier, M.Sc. thesis, University of Ottawa, 2006.
[33] S. J. Marrink, R. M. Sok, and H. J. C. Berendsen, J. Chem. Phys. **104**, 9090 (1996).
[34] D. Boal, *Mechanics of the Cell* (Cambridge University Press, Cambridge, 2002).
[35] S. J. Marrink and A. E. Mark, J. Phys. Chem. B **105**, 6122 (2001).
[36] G. Cevc and D. Marsh, *Phospholipid Bilayers: Physical Principles and Models* (Wiley-Interscience, New York, 1987).